

MODAL ANALYSIS OF ELECTROMAGNETIC COUPLING BETWEEN SMA-FEEDTHROUGH ELECTRODE AND BEAM FOR WIDEBAND BEAM MONITOR

T. Suwada*, High Energy Accelerator Research Organization (KEK),
also at SOKENDAI (The Graduate University for Advanced Studies), Tsukuba, Japan

Abstract

The direct simultaneous detection of electron (e^-) and positron (e^+) bunch signals was successfully performed for the first time by a wideband beam monitor at the e^+ capture section of the SuperKEKB factory. This monitor can measure a time interval between the e^- and e^+ bunches, their bunch lengths, bunch intensities, and transverse beam positions, depending on the phase of accelerating structures. For this purpose, a new beam monitor with wideband pickups simply using SMA feedthroughs and a wideband detection system based on a real-time oscilloscope was developed to investigate their capture process at the capture section and to maximally optimize the e^+ intensity. The required specification for the new monitor is to simultaneously detect the e^+ and e^- bunches generated in the capture section within the resolution of pico-second level with a sufficient dynamic range in the time-interval and bunch-length measurements. In this report, the basic design and numerical results based on a modal analysis of electromagnetic couplings between SMA-feedthrough and beam are in detail given.

INTRODUCTION

The SuperKEKB B-factory [1] (SKEKB) is a next-generation B-factory that is currently in operation at KEK, after the KEK B-factory [2] (KEKB) was discontinued in 2010. The SKEKB is a e^+e^- collider with asymmetric energies; it comprises 4 GeV e^+ (LER) and 7 GeV e^- (HER) rings. The target luminosity ($8 \times 10^{35} \text{ cm}^{-2}\text{s}^{-1}$) of the SKEKB, that is, the rate of e^- and e^+ collisions, is 40 times the peak luminosity of the KEKB. To improve the collision rate, the development of a powerful and stable e^+ source is one of the key elements in this experiment. The SKEKB injector linac [3] is an e^-/e^+ linear accelerator for the SKEKB; the KEKB injector linac [4] was upgraded for the abovementioned purpose. The requirements for the injector linac are full energy injection into the SKEKB rings with the e^- and e^+ bunch charges of 5 and 4 nC, respectively. The injector linac should deliver high-current e^+ beams to the SKEKB. The e^+ production and capture section are described in detail elsewhere [3].

Since both the electrons and positrons with approximately equivalent amounts of bunch charges are generated at the target, not only the positrons but also the electrons are simultaneously captured and accelerated (or decelerated) in the capture section with a certain time interval that is dependent on the operational condition of the capture section. The time

interval between the e^- and e^+ bunches is very short with a time range from 135 to 265 ps.

The time interval between the e^- and e^+ bunches, their bunch lengths and intensities for each e^- and e^+ bunch are very important parameters that can be fundamentally investigated on the basis of detailed beam dynamics at the capture section. However, they have never been measured because the time interval is too short to detect them independently, while they are generally simulated on the basis of beam dynamics in multidimensional transverse and longitudinal phase spaces. Thus, it is a challenging to experimentally verify and elucidate complicated beam dynamics for both positrons and electrons in the capture section in order to fully understand them and to maximize the e^+ intensity under an optimized operation condition.

For this purpose, new beam monitors with not only wideband pickups but also a wideband detection system were installed at the capture section to simultaneously detect e^- and e^+ signals during the summer shutdown of 2019. They are essential diagnostic instruments to fully investigate the e^- and e^+ capture process and to maximally optimize the e^+ intensity. Both the electrons and positrons generated at the target are formed into their steady bunched beams through their phase slip process in accelerating structures of the capture section. Thus, the experimental tests were successfully carried out at the e^+ capture section of the injector linac [5].

In this report a very wideband beam monitor with SMA-feedthroughs has been designed, and the modal analysis of electromagnetic coupling between SMA-feedthrough and beam is described on the basis of analytical methods with electromagnetic couplings between two coaxial structures.

WIDEBAND BEAM MONITOR SYSTEM

Mechanical Structure

A photo picture of the wideband beam monitor is shown in Fig. 1.

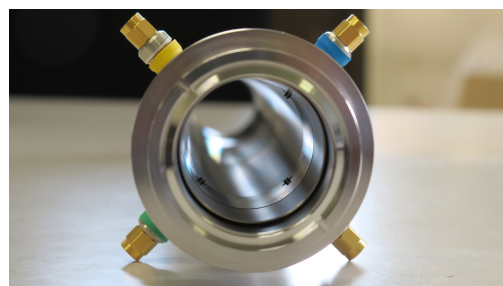


Figure 1: Photograph of the new beam monitor.

* tsuyoshi.suwada@kek.jp

The total length of the monitor including two bellows and quick-release flange couplings (KFS-NW40, EVAC AG) at both ends is 431 mm, and the inner diameter is 38 mm. The inner surface of the front bellows is covered with a cylindrical pipe to remove the irregularity in order to suppress any wakefield effects caused at the monitor front as much as possible. The pickups of the monitor are made of SMA-type vacuum feedthroughs composed of a central conductor pin made of Kovar and a dielectric substance made of ceramic. The pickups have good frequency characteristics, which were tested in the frequency region greater than 10 GHz. The four pickups, two horizontal and two vertical, are mounted on the upstream of the monitor with $\pi/2$ rotational symmetry. Thus, this monitor can also work as beam position monitor (BPM). The tips of the center pins protrude for a length of 1 mm toward the monitor center from the inner surface of the monitor in order to have its good frequency response.

Signal Detection System

A schematic drawing of the signal detection system is shown in Fig. 2.

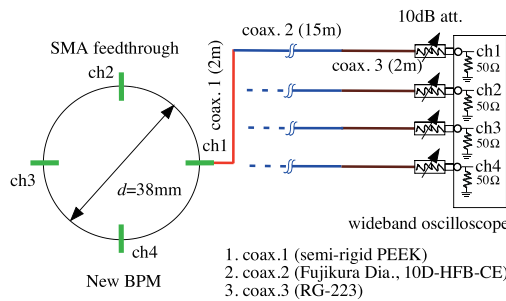


Figure 2: Signal detection system of the new monitor.

The beam signal can be detected with four SMA feedthrough electrodes and the four signals are sent directly to a wideband oscilloscope with four channels through 10-dB attenuator in front of each channel. One coaxial cable comprises 2m-long semirigid coaxial with its insulator of polyether ether ketone ($\epsilon_r = 3.5$), 15m-long 10D coaxial cable, and 2m-long RG223 cable. The total length of the coaxial is 19 m. The maximum operating frequency is limited at 10 GHz, which is the cutoff frequency of lowest TE mode for the 10D cable.

ELECTROMAGNETIC COUPLING ANALYSIS

Detection Principle

It may be instructive to describe fundamental electromagnetic couplings between two coaxial structures before the coupling between beam and SMA feedthrough. We consider SMA and another coaxial structure as shown in Fig. 3 (a).

If the SMA is excited by an external rf source, the coaxial tube is excited through electromagnetic coupling, which can be in detail described based on a coupling scheme between two coaxial structures [6]. The fundamental TEM and

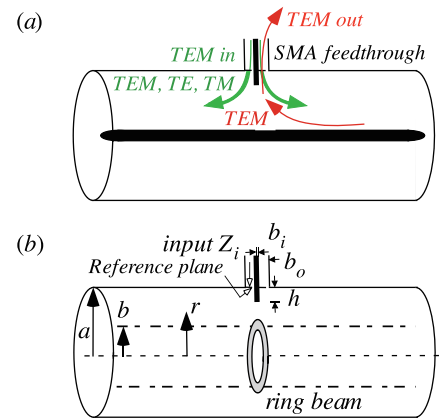


Figure 3: (a) Schematic drawing of electromagnetic couplings between SMA feedthrough and coaxial structure. (b) Electromagnetic couplings between SMA feedthrough and a thin ring beam. Inner radius of the coaxial structure: $a = 19$ mm, ring-beam radius: b , radii of the SMA inner and outer conductor: $b_i = 0.9$ mm, $b_o = 2.05$ mm, and the characteristic impedance of the SMA is $Z_0 = 50 \Omega$.

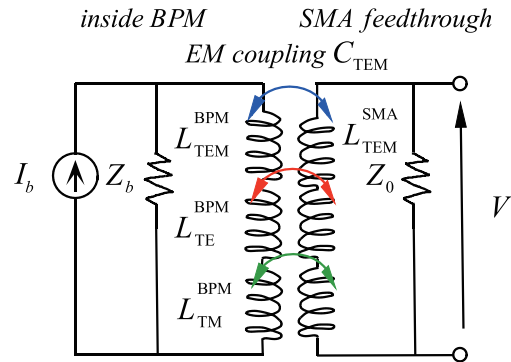


Figure 4: Equivalent circuit of electromagnetic couplings between SMA feedthrough and coaxial structure. The arrows indicate the couplings between TEMs (blue), TE and TEM (red), and TM and TEM (green).

also higher-order TE and TM modes are excited in the coaxial tube at a reference plane defined as a boundary surface between the SMA and coaxial tube, if the excited electromagnetic fields are viewed at the reference plane to the direction of rf transmission from the SMA to the coaxial tube. If the coaxial tube is excited, it can be understood that these higher-order modes are excited at the reference plane in the time reversal process. However, the higher-order modes cannot transmit directly to the SMA due to its higher cut-off frequency. It is thus enough to take into account only the TEM couplings between two coaxial structures, while slight parts of the higher-order modes may be transformed to fundamental TEM at the reference plane. Thus, a scheme is shown by an equivalent circuit with taking into account electromagnetic couplings as shown in Fig. 4.

Based on such a coupling scheme, the coaxial tube may be replaced by a sufficiently thin ring beam, because the equivalent current flow in the coaxial tube is limited on the

outer surface of the inner rod. Thus, the coupling between two coaxial structures is equivalent to that between SMA feedthrough and beam. If a gaussian beam in the transverse directions is taken into account, by appropriate integration in the transverse directions, the coupling strength can be numerically calculated.

ANALYTICAL FORMULATION

If SMA feedthrough is excited by an external rf source, TEM excited in a coaxial tube is represented by

$$E_{r_0}(r) = \frac{1}{\sqrt{\ln(a/b)}} \frac{1}{r}, \quad E_{\phi_0}(r) = 0. \quad (1)$$

The higher-order TEs are represented by

$$E_{r_{mn}}(r) = \frac{\sqrt{\pi}(m/r)[J_m(kc_{mn}r)N'_m(kc_{mn}b) - N_m(kc_{mn}r)J'_m(kc_{mn}b)]}{\sqrt{(J'_m(kc_{mn}b)/J'_m(kc_{mn}a))^2 [1 - (m/kc_{mn}a)^2] - [1 - (m/kc_{mn}b)^2]}}, \quad (2)$$

$$E_{\phi_{mn}} = \frac{\sqrt{\pi}(kc_{mn})[J'_m(kc_{mn}r)N'_m(kc_{mn}b) - N'_m(kc_{mn}r)J'_m(kc_{mn}b)]}{\sqrt{(J'_m(kc_{mn}b)/J'_m(kc_{mn}a))^2 [1 - (m/kc_{mn}a)^2] - [1 - (m/kc_{mn}b)^2]}}, \quad (3)$$

$$E_{r_{mn}}(\phi) = \sin(m\phi), \quad E_{\phi_{mn}}(\phi) = \cos(m\phi). \quad (4)$$

Here, E_r and E_ϕ are the excited electric fields in the radial and angular directions, respectively. The subscripts 0 and mn mean those for TEM and TE modes, respectively. $f_c(m, n)$ and kc_{mn} are the cutoff frequency and wave length for TE modes, respectively. $J_m(z)$ and $N_m(z)$ are Bessel and Neumann functions, respectively. $J'_m(z)$ and $N'_m(z)$ are derivatives on z for Bessel and Neumann functions, respectively. X'_{mn} are roots of Bessel-Neumann combined function [7]. This relation is given by

$$af_c(m, n) = \frac{c_0 X'_{mn}}{2\pi(b/a)}, \quad X'_{mn} = kc_{mn}b. \quad (5)$$

By applying these formulation, the impedances for TEM, TE and TM modes are given by

$$Z^{TEM} = \frac{\eta_0}{2\pi} \left[\int_{a-h}^a I(r) E_{r_0}(r) dr \right]^2, \quad (6)$$

$$Z^{TE}_{mn} = \frac{\eta_{mn}}{2\pi\sigma} \frac{\int_{a-h}^a I(r) E_{r_{mn}}(r) dr}{\int_a^b [E_{r_{mn}}^2(r) + E_{\phi_{mn}}^2(r)] r dr} \times \int_{a-h}^a I(r) E_{r_{mn}}(r) F_{mn}(r, b_i) dr, \quad (7)$$

$$Z^{TM}_{mn} = \frac{-jm^2 \eta_{mn}}{2\pi\sigma} \frac{\int_{a-h}^a I(r) E_{r_{mn}}(r) dr}{\int_a^b r^3 E_{\phi_{mn}}^2(r) dr} \times \int_{a-h}^a I(r) E_{r_{mn}}(r) F_{mn}(r, b_i) dr. \quad (8)$$

$$\eta_{mn} = \frac{\eta_0}{\sqrt{1 - (kc_{mn}/\beta_0)^2}}, \quad \eta_0 = \sqrt{\frac{\mu_0}{\epsilon_0}} = 376.7 (\Omega), \quad (9)$$

$$I(r) = \frac{\sin[\beta_0(h+r-a)]}{\sin(\beta_0 h)}, \quad (10)$$

$$F_{mn}(r) = \frac{1}{2\pi} \int_0^{2\pi} e^{-\gamma_{mn} b_i |\sin \theta|} \cos \left[m \cdot \tan^{-1} \left(\frac{b_i \cos \theta}{r} \right) \right] d\theta. \quad (11)$$

Here, h is the extruding length of the SMA feedthrough from the inner surface of BPM, η_0 the wave impedance in vacuum, η_{mn} the intrinsic impedance transmitted in BPM, β_0 the phase constant in vacuum, γ_{mn} the propagation constant of TE and TM modes, σ a constant by $\sigma = 1/2$ for $m > 0$ and

$\sigma = 1$ for $m = 0$, ϵ_0 and μ_0 are permittivity and permeability in vacuum, respectively. $I(r)$ a normalized current excited in BPM, which is a function of the radius r of BPM. F_{mn} is the attenuation function of the excited electromagnetic fields in BPM as a function of r with taking into account the geometrical structure of the SMA feedthrough.

Based on these formulation, the input (output) impedance Z_{in} (Z_{out}) viewed the reference plane from the SMA (BPM) side to the BPM (SMA) side can be represented by

$$Z_{in} = \frac{1}{2} \left[Z_{TEM} + \sum_{m=1}^{\infty} \sum_{n=1}^{\infty} Z_{TE_{mn}} + \sum_{m=0}^{\infty} \sum_{n=1}^{\infty} Z_{TM_{mn}} \right], \quad (12)$$

$$Z_{out} = Z_{TEM}. \quad (13)$$

Here, in Eq. (12), the factor 1/2 corresponds to a junction of the excited current at the reference plane in the directions of both upstream and downstream of BPM. On the other hand, when BPM is excited in one-way direction, this factor does not need to be taken into account.

If a gaussian beam in the transverse directions is taken into account, based on appropriate integration in the transverse directions, the input impedance can be numerically calculated. In the calculations, the integration region is taken into account $3\sigma_b$ ($r \leq a$) or the limit a ($r > a$), where σ_b is one sigma of the gaussian beam. Figure 5 shows the results of the input impedance calculation. Fig. 5 (a) ((b)) indicates the variation in the input impedance (TEM and TE (TM) modes) as a function of frequency and the beam size. Gaussian function is assumed in the transverse charge distribution. It is easily understood that Z_{TEM} does not depend on frequency, and the higher-order modes arise in order at their corresponding cutoff frequencies starting from their lowest order. Note that the input impedances of TE (TM) modes are $7 \times 10^{-3} \sim 5 \times 10^{-2} \Omega$ ($7 \times 10^{-3} \sim 2 \times 10^{-2} \Omega$) depending on frequency and beam size. It is easily understood that the input impedance of TE mode is larger than those of TM mode.

Coupling Strength Between SMA Feedthrough and Beam

If the BPM is excited by a beam with a unit current, the coupling strength C_{TEM} between a beam and SMA feedthrough with taking into account only fundamental TEMs is given by

$$C_{TEM} = \frac{Z_{out}}{Z_{BPM}}, \quad Z_{BPM} = \frac{\eta_0}{2\pi} \ln(a/b). \quad (14)$$

Figure 6 shows the variations in the coupling strength as a function of frequency and the beam size with taking into account a gaussian beam in the transverse direction. It is expected $C_{TEM} \sim 7 \times 10^{-4}$ in a case of $\sigma_b = 6$ mm. The result shows that in a case of bunch currents of ~ 1 kA, which corresponds to beam charges of 1 nC for a single bunch, ~ 0.7 A is expected to be excited at the reference plane of SMA feedthrough. The amplitude of ~ 35 V is expected to be detected in a 50 Ω transmission system. This amplitude is sufficiently detectable in the SKEKB e^+ capture section.

Figure 7 shows the variations in the coupling strength as a function of frequency and the extruding length h at the beam

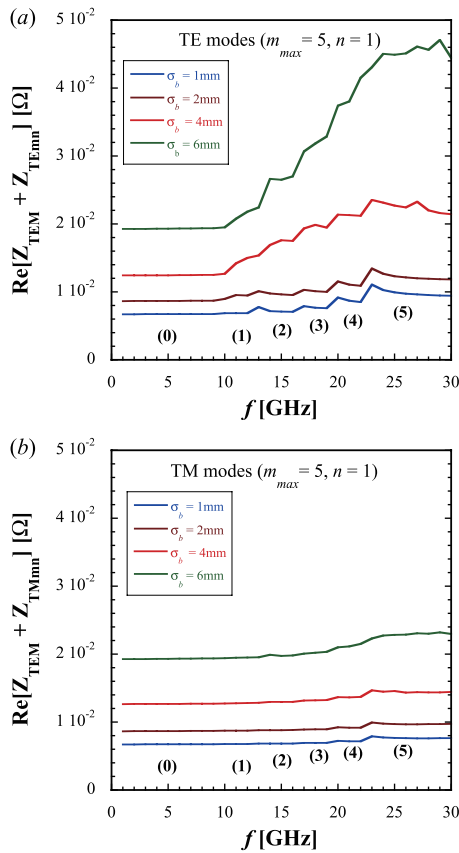


Figure 5: (a) Variations in the input impedance (TEM and TE modes) as a function of frequency and the beam size, (b) Variations in that (TEM and TM modes) as a function of frequency and the beam size. The subscripts n and maximum m are fixed to 1 and 5, respectively. The extruding length h is fixed to 1 mm.

size of $\sigma_b = 4$ mm. Note that with increasing the extruding length, the coupling strength increases as a function of frequency and also beam size, while the frequency dependence of the coupling strength increases. In our present design, the length is $h = 1$ mm, and thus, the variation of it is $\sim 0.7\%$ in the frequency region up to 10 GHz. It is understood that the variation of the coupling strength is negligibly small.

CONCLUSION

The basic design and numerical results based on a modal analysis for electromagnetic couplings between SMA-feedthrough electrode and a beam are successfully investigated. Based on the design parameters, it was verified that the wideband monitor system can work well in the direct simultaneous detection of e^- and e^+ bunches.

REFERENCES

[1] Y. Ohnishi *et al.*, “Accelerator design at SuperKEKB”, *Prog. Theor. Exp. Phys.*, vol. 2013, p.03A011, 2013. doi:10.1093/ptep/pts083

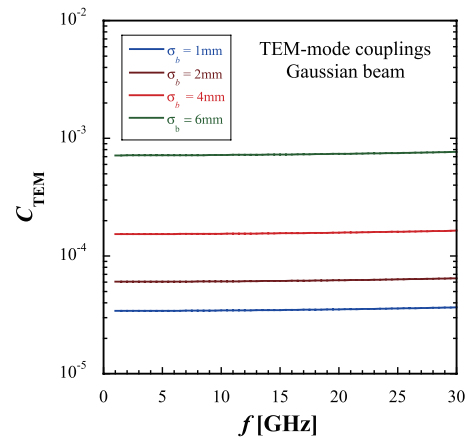


Figure 6: Variations in the coupling strengths between the TEM modes as a function of frequency and the beam size.

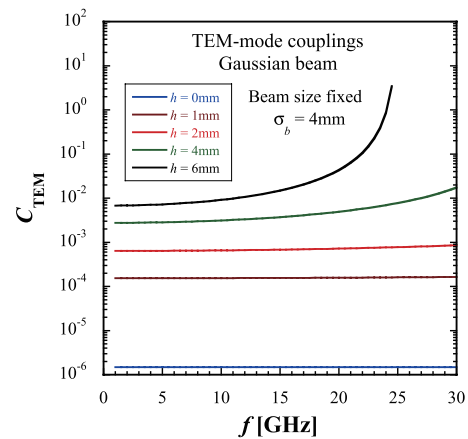


Figure 7: Variations in the coupling strengths between the TEM modes as functions of frequency and the length h . The transverse charge distribution of $\sigma_b = 4$ mm is fixed.

[2] T. Abe *et al.*, “Achievements of KEKB”, *Prog. Theor. Exp. Phys.*, vol. 2013, p. 03A001, 2013. doi:10.1093/ptep/pts102

[3] M. Akemoto *et al.*, “The KEKB injector linac”, *Prog. Theor. Exp. Phys.*, vol 2013, p. 03A002, 2013. doi:10.1093/ptep/ptt011

[4] I. Abe *et al.*, “The KEKB injector linac”, *Nucl. Instrum. Methods Phys. Res. A*, vol. 499, p. 167, 2003. doi:10.1016/S0168-9002(02)01787-4

[5] T. Suwada, M. A. Rehman, and F. Miyahara, “First simultaneous detection of electron and positron bunches at the positron capture section of the SuperKEKB factory”, *Sci. Rep.*, vol. 11, p. 12751, 2021. doi:10.1038/s41598-021-91707-0

[6] J. G.Davis and A. A. P. Gibson, “Higher order mode impedances and cut-off frequencies of overmoded coaxial waveguides”, *Int. J. Electron.*, vol. 93, no. 5, pp. 335–346, 2006. doi:10.1080/00207210500429077

[7] N. Marcuvitz, *Waveguide Handbook*, Peter Peregrinus Ltd., UK, 1986, p. 74.